

# Technical Note: A software framework for calculating compositionally dependent *in situ* $^{14}\text{C}$ production rates

Alexandria J. Koester<sup>1</sup>, Nathaniel A. Lifton<sup>1,2</sup>

<sup>1</sup>Department of Earth, Atmospheric, and Planetary Sciences, Purdue University, West Lafayette, IN 47907, USA

5 <sup>2</sup>Department of Physics and Astronomy, Purdue University, West Lafayette, IN 47907, USA

Correspondence to: Alexandria J. Koester (koestea@purdue.edu)

## Abstract

Over the last 30 years, *in situ* cosmogenic nuclides (CNs) have revolutionized surficial process and Quaternary geologic  
10 studies. Commonly measured CNs extracted from the common mineral quartz have long half-lives (e.g.,  $^{10}\text{Be}$ ,  $^{26}\text{Al}$ ), and have  
been applied over timescales from a few hundred years to millions of years. However, their long half-lives also render them  
largely insensitive to complex histories of burial and exposure less than ca. 100 ky. On the other hand, *in situ* cosmogenic  $^{14}\text{C}$  (*in*  
*situ*  $^{14}\text{C}$ ) is also produced in quartz, yet its 5.7 ky half-life renders it very sensitive to complex exposure histories during the last  
~25 ka – a particularly unique and powerful tool when analyzed in concert with long-lived nuclides. *In situ*  $^{14}\text{C}$  measurements  
15 are currently limited to relatively coarse-grained (typically sand-sized or larger, crushed/sieved to sand) quartz-bearing rock  
types, but while such rocks are common, they are not ubiquitous. The ability to extract and interpret *in situ*  $^{14}\text{C}$  from quartz-poor  
and fine-grained rocks would thus open its unique applications to a broader array of landscape elements and environments.

As a first step toward this goal, a robust means of interpreting *in situ*  $^{14}\text{C}$  concentrations derived from rocks and minerals  
spanning wider compositional and textural ranges will be crucial. We have thus developed a MATLAB<sup>®</sup>-based software  
20 framework to quantify spallogenic production of *in situ*  $^{14}\text{C}$  from a broad range of silicate rock and mineral compositions,  
including rocks too fine-grained to achieve pure quartz separates. As expected from prior work, production from oxygen  
dominates the overall *in situ*  $^{14}\text{C}$  signal, accounting for >90% of production for common silicate minerals and six different rock  
types at sea-level and high latitudes (SLHL). This work confirms that Si, Al, and Mg are important targets, but also predicts  
greater production from Na than from those [target elements](#). The compositionally dependent production rates for rock and  
25 mineral compositions investigated here are typically lower than that of quartz, although that predicted for albite is comparable to  
quartz, reflecting the significance of production from Na. Predicted production rates drop as compositions become more mafic  
(particularly Fe-rich). This framework should thus be a useful tool in efforts to broaden the utility of *in situ*  $^{14}\text{C}$  to quartz-poor  
and fine-grained rock types, but future improvements in measured and modelled excitation functions would be beneficial.

## 1 Introduction

30 Rare nuclides produced *in situ* in minerals near the Earth's surface by cosmic-ray bombardment (*in situ* cosmogenic nuclides  
or CNs) have revolutionized studies of geomorphology and Quaternary geology. CNs build predictably over time in an exposed  
surface through nucleon spallation and muon reactions (e.g., Gosse and Phillips, 2001). As such, the time at which geomorphic  
surfaces formed by glacial, fluvial, or marine activity often can be constrained with CNs, an application known as surface  
exposure dating. In addition, CNs can be used to constrain rates of surficial processes with appropriate interpretive models.  
35 These applications rely on measuring the concentrations (atoms  $\text{g}^{-1}$ ) of CNs in a sample and calculating an exposure age or

erosion rate based on the production rate (atoms  $\text{g}^{-1} \text{yr}^{-1}$ ). The most-commonly measured CNs,  $^{10}\text{Be}$  and  $^{26}\text{Al}$  ( $t_{1/2}$  1.39 My - Korschinek et al. (2010); Chmeleff et al. (2010); and  $t_{1/2}$  0.705 My - Nishiizumi et al. (2004), respectively), are typically extracted from quartz, due to its simple composition and corresponding resistance to weathering under a wide range of environmental conditions. Their long half-lives make these nuclides useful in dating surfaces that have been exposed up to millions of years. However, their half-lives also render their concentrations insensitive to periods of burial and re-exposure of less than ca. 100 ky – this can lead to problems with exposure dating due to nuclide inventories remaining from prior periods of exposure.

*In situ* cosmogenic  $^{14}\text{C}$  (*in situ*  $^{14}\text{C}$ ) is also produced in quartz, but its 5.7 ky half-life limits its utility for simple exposure dating because its concentration reaches secular equilibrium between production and decay after 25-30 ky of continuous exposure. However, its rapid decay also makes it sensitive to complex periods of burial and exposure since ca. 25-30 ka (e.g., Briner et al., 2014). In addition, its short half-life means measured concentrations are sensitive only to very rapid erosion rates (e.g., Gosse and Phillips, 2001; von Blanckenburg et al., 2005; Hippe et al., 2017; Hippe et al., 2021), making many eroding landscape elements good targets for *in situ*  $^{14}\text{C}$  studies. *In situ*  $^{14}\text{C}$  is thus emerging as a powerful addition to the CN toolkit.

Several techniques for extracting *in situ*  $^{14}\text{C}$  from sand-sized quartz grains have been established (Lifton et al., 2001; Lifton et al., 2015; Goehring et al., 2019; Hippe et al., 2013; Lupker et al., 2019; Fülöp et al., 2019), but while coarse-grained quartz is common, it is not ubiquitous. Landscapes dominated by mafic or intermediate lithologies generally lack quartz, and fine-grained lithologies can limit the efficacy of quartz purification techniques; thus applying *in situ*  $^{14}\text{C}$  to such rock types is currently problematic. However, the ability to extract and interpret *in situ*  $^{14}\text{C}$  concentrations reliably from quartz-poor and fine-grained lithologies would significantly broaden its applications to additional landscapes and enable pairing with additional nuclides such as  $^{36}\text{Cl}$ . Indeed, early studies of *in situ*  $^{14}\text{C}$  in terrestrial rocks utilized whole-rock samples (e.g., Jull et al., 1992; 1994), until procedural difficulties shifted the focus to the simpler quartz production and extraction systematics (Lifton, 1997; Lifton et al., 2001).

As a first step in expanding the range of available sample targets, we have developed a software framework that estimates the production of *in situ*  $^{14}\text{C}$  from major elements found in typical rocks and potential mineral separates. We modified the MATLAB® code from Lifton et al. (2014) to calculate compositionally dependent, site-specific production rates using nuclide-specific scaling, major-element oxide compositions, and measured and modelled nucleon excitation functions, referenced to geologically calibrated *in situ*  $^{14}\text{C}$  spallogenic production rates in quartz. [Anticipating that appropriate extraction and  \$\text{CO}\_2\$  purification procedures can be developed](#), this new framework thus provides a critical first step for potential future applications incorporating quartz-poor or fine-grained samples.

## 2 Constraining compositionally dependent *in situ* $^{14}\text{C}$ production rates

### 2.1 Geologic and experimental production rate calibrations

*In situ* CN applications require accurate estimates of the rate at which a given nuclide of interest is produced in the target mineral or rock. This is typically achieved by calibrating the production rate with CN measurements in samples from one or more sites with 1) an independently well-constrained exposure history (e.g., Borchers et al., 2016; Phillips et al., 2016; Lifton et al., 2015a), or for radionuclides only, with 2) demonstrable surface stability such that measured CN concentrations can be inferred to have reached a secular equilibrium between production and decay, at which point the concentration is only a function

of time-integrated production rate and the decay constant (e.g., Jull et al., 1992; Borchers et al., 2016). Production rates can also be calibrated experimentally by exposing high-purity, low background targets to the secondary cosmic-ray flux at given sites for a known duration under well-constrained conditions (e.g., Nishiizumi et al., 1996; Brown et al., 2000; Vermeesch et al., 2009).

75 Since production rates cannot be calibrated at every place on Earth, these site-specific estimates are typically scaled to other sites of interest using an appropriate scaling framework that accounts for spatial and temporal variations in the secondary cosmic-ray flux, arising from fluctuations in the geomagnetic field (parameterized by effective vertical cutoff rigidity,  $R_C$ , in GV), atmospheric depth ( $X$ , in  $\text{g cm}^{-2}$ ), and solar modulation (described by the parameter  $\Phi$ , in MeV) (e.g., Lifton et al., 2014). Such scaling frameworks are typically referenced to conditions corresponding to sea-level and high geomagnetic latitude  
80 (SLHL).

Geologic calibrations are generally preferable for minerals with specific compositions since samples from sites with [independently](#) well-constrained exposure histories should incorporate natural [geologic](#) variability relevant over geologic time spans. Such calibrations for *in situ*  $^{14}\text{C}$  have focused on quartz to date, given its simple chemistry and weathering resistance, [as noted above](#) (e.g., Borchers et al., 2016; Phillips et al., 2016; Lifton et al., 2015a; Schimmelpfennig et al., 2012; Young et al.,  
85 2014), yet variable compositions require more complicated consideration of the compositional dependence of CN production (e.g.,  $^{36}\text{Cl}$ ; Marrero et al., 2016a). It is often useful in such cases to utilize theoretical production rate estimates based on integrals of the differential cosmic-ray flux and the relationship between reaction probability and incident particle energy.

## 2.2 Theoretical production rate estimates

The probability that a given nuclear reaction will occur at a given kinetic energy  $E$  of an incident particle is described by the  
90 reaction cross-section ( $\sigma$ ), in units of barns ( $1 \text{ barn} = 10^{-24} \text{ cm}^2$ ). With the advent of accelerator mass spectrometry (AMS), cross-section measurements for reactions producing CNs have become relatively common, and knowledge of the variation of  $\sigma$  as a function of  $E$  for those reactions (known as an excitation function) are continuing to improve (e.g., Reedy, 2013). Proton-induced reactions are simpler to measure than those induced by neutrons because it is easier to accelerate protons into a mono-energetic beam. Mono-energetic (or quasi-mono-energetic) neutron reaction cross-sections are more difficult to obtain, however,  
95 and thus are often estimated from analogous proton cross-sections (Reedy, 2013).

Measured or modelled excitation functions can then be used to estimate theoretical production rates for a CN of interest using Eq. (1) below (e.g., Masarik and Beer, 2009),

$$P_j(X, R_C, \Phi) = \sum_i ND_i \sum_k \int_0^\infty \sigma_{ijk}(E_k) J_k(E_k, X, R_C, \Phi) dE_k \quad (1)$$

where  $ND_i$  is the target number density, or number of atoms of the target element  $i$  per gram of sample material ( $\text{atoms g}^{-1}$ ),  
100  $\sigma_{ijk}(E_k)$  is the cross-section for the production of nuclide  $j$  ( $\text{cm}^2$ ) by particles of type  $k$  with energy  $E_k$  (MeV), and  $J_k(E_k, X, R_C, \Phi)$  is the differential flux of atmospheric cosmic-ray particles ( $\text{cm}^{-2} \text{ yr}^{-1} \text{ MeV}^{-1}$ ) of type  $k$  with energy  $E_k$  at a location and time specified by  $X$ ,  $R_C$ , and  $\Phi$ .

The production of *in situ*  $^{14}\text{C}$  in silicates is dominantly from spallation of O, and theoretical simulations suggest minor spallogenic production from Mg, Al, and Si (Masarik and Reedy, 1995; Masarik, 2002). Production of *in situ*  $^{14}\text{C}$  from muons  
105 also occurs, either via slow negative muon capture or by fast muon interactions (Heisinger et al., 2002a,b). The muogenic component of *in situ*  $^{14}\text{C}$  production in surficial quartz at SLHL is significant – on the order of 20% of total production (e.g., Lupker et al., 2015; Balco, 2017). However, muogenic production of *in situ*  $^{14}\text{C}$  has only been estimated experimentally from

$^{16}\text{O}$  (Heisinger et al., 2002a; 2002b). Further work is needed in this area to better understand production from other muogenic reactions. We therefore focus on the dominant spallogenic pathways for the purposes of this initial study.

## 110 3 Methods

### 3.1 Software framework

Our MATLAB<sup>®</sup>-based compositionally dependent *in situ*  $^{14}\text{C}$  production rate software framework builds on the LSDn nuclide-dependent scaling formulation of Lifton et al. (2014), which uses the PARMA analytical approximations to Monte Carlo calculations of atmospheric differential flux spectra of neutrons, protons, and muons as a function of  $X$ ,  $R_C$ , and  $\Phi$  (Sato et al., 115 2006; 2008). We also incorporate the time-dependent gridded  $R_C$  (global grids of cutoff rigidity) and dipolar  $R_{CD}$  (geocentric dipolar cutoff rigidity) models of Lifton et al. (2016), based on the SHA.DIF.14k paleomagnetic model (Pavón-Carrasco et al., 2014). This work accounts for effects of variable sample compositions on *in situ*  $^{14}\text{C}$  production by incorporating relevant reaction excitation functions and number densities for elements in the standard suite of major-element oxide compositions. Output from this new framework should complement current web-based cosmogenic nuclide calculators incorporating the LSDn 120 scaling framework and *in situ*  $^{14}\text{C}$ , including version 3 of the University of Washington cosmogenic-nuclide calculators (herein UWv3: hess.ess.washington.edu) (Balco et al., 2008) and the Cosmic-Ray-produced NUclide Systematics on Earth project (CRONUS-Earth) calculator (CRONUSCalc; <http://cronus.cosmogenicnuclides.rocks/>; Marrero et al., 2016b).

Reaction excitation functions for neutrons and protons were compiled from Reedy (2007; 2013), and the JENDL/HE-2007 database (Fukahori et al., 2002; Watanabe et al., 2011) found in the online Evaluated Nuclear Data File (ENDF, [https://www- 125 nds.iaea.org/exfor/endl.htm](https://www-nds.iaea.org/exfor/endl.htm), accessed April 2020; Brown et al., 2018) for each of the major elements included in typical elemental oxide analyses. We consider empirical excitation functions to be generally more reliable than those derived from nuclear reaction models, and thus use measured functions if available. Five neutron and proton excitation functions are based on measurements from Reedy (2007, 2013) of [elements at](#) natural isotopic abundances (O, Mg, Al, Si, Fe), while we used modelled neutron and proton reaction excitation functions from JENDL/HE-2007 for [the most abundant isotopes of](#) the remaining 130 elements [considered](#) ( $^{23}\text{Na}$ ,  $^{31}\text{P}$ ,  $^{39}\text{K}$ ,  $^{40}\text{Ca}$ ,  $^{48}\text{Ti}$ ,  $^{55}\text{Mn}$ ). ~~However, we not~~ [Apart from the measured excitation function for \*in situ\*  \$^{14}\text{C}\$  production by neutron spallation from oxygen \(Reedy, 2013\), e-that it is important to note that most of the Reedy \(2007, 2013\) neutron excitation functions are not directly measured but instead are represented by Reedy \(2013\) are derived from the measured proton excitation functions. We utilized the JENDL/HE-2007 database because the relevant excitation functions extended to a maximum energy of 3 GeV, \[close to the maximum 10 GeV energy considered by Sato et al. \\(2006, 2008\\); a 135 version of that nuclear data library was also utilized by those studies.\]\(#\) The exceptions were the excitation functions for  \$^{31}\text{P}\$ , extending only to 0.2 GeV. Each excitation function was interpolated into logarithmic energy bins from 1 MeV to 200 GeV for both neutron \( \$\text{XX}\(\text{n},\text{x}\)^{14}\text{C}\$ \) and proton \( \$\text{XX}\(\text{p},\text{x}\)^{14}\text{C}\$ \) reactions, where XX is the target nuclide \(Fig. 1\). The cross-section at the highest measured or modelled energy reported for each excitation function is assumed to be constant beyond that energy up to 200 GeV, the maximum energy we consider.](#)

140 We incorporate sample compositions using common major elemental oxide analyses (e.g., from X-Ray Fluorescence (XRF) measurements) to calculate ND for each element considered in Eq. 1. The ND value for each target element in a sample is then calculated per Eq. (2), for input to Eq. 1:

$$ND = \frac{E_{Fr} * E_{Ox} * N_A}{100 * A_m}, \quad (2)$$

where  $E_{Fr}$  is the elemental fraction in each oxide (formula mass of each element in its oxide divided by the total formula mass of the oxide (e.g., Mg/MgO or 2Al/Al<sub>2</sub>O<sub>3</sub>)),  $E_{Ox}$  is the measured major elemental oxide weight percent input by the user,  $N_A$  is Avogadro's number ( $6.02214076 \times 10^{23}$  atoms mol<sup>-1</sup>) and  $A_m$  is the molar mass of the element in g. This approach [is applicable to works for](#) any silicate major elemental oxide composition input by the user.

### 3.2 Predicted compositionally dependent production rates

Theoretical compositionally dependent site-specific *in situ* <sup>14</sup>C production rates are reported relative to the SLHL *in situ* <sup>14</sup>C [global](#) production rate in quartz, geologically calibrated as part of the CRONUS-Earth project (e.g., [Borchers et al. 2016](#); Phillips et al., 2016; [Borchers et al., 2016](#)) and supplemented with two subsequent production rate calibration datasets (Schimmelpfennig et al., 2012; Young et al., 2014), using the LSDn scaling framework (Lifton et al., 2014, Lifton 2016) ([Supplemental Information Table S1](#)). [All \*in situ\* <sup>14</sup>C measurements in these studies were recalculated following Hippe and Lifton \(2014\).](#) SLHL estimates are referenced to the year 2010 (Lifton et al., 2014; Lifton, 2016) assuming an atmospheric pressure of 1013.25 hPa (converted to atmospheric depth, g cm<sup>-2</sup>), an  $R_c$  value of 0 GV, a  $\Phi_{2010}$  value of 624.5718 MV, and a fractional water content value, 'w', of 0.066 (Sato et al., 2006; Phillips et al. 2016). We recalibrated the *in situ* <sup>14</sup>C spallogenic production rate at SLHL in quartz from the studies above by first calculating the unweighted mean and standard deviation of replicate analyses of samples at each site (to avoid biasing the results toward sites with more analyses). Best-fitting SLHL production rate estimates for each site were determined using a  $\chi^2$  minimization procedure. The unweighted mean and standard deviation of all sites were then calculated from the site-specific SLHL production rate estimates, yielding global SLHL values for quartz of  $13.5 \pm 0.9$  atoms g<sup>-1</sup> yr<sup>-1</sup> and  $13.7 \pm 1.2$  atoms g<sup>-1</sup> yr<sup>-1</sup> for the gridded  $R_c$  and geocentric dipolar  $R_{CD}$  records of Lifton (2016), respectively, as noted above. The latter is comparable to the calibrated value generated by the UWv3 calculator from the same dataset ([Table S1](#)). In the following discussion we focus on the gridded  $R_c$  value (referenced below as  $P_{Qcal}$ ), as it provides a somewhat better fit to the global calibration dataset. Corresponding geocentric dipolar values are included in the [SupplementTable S2](#).

For comparison, the purely theoretical *in situ* <sup>14</sup>C production rate by nucleon spallation predicted at SLHL in quartz using Eq. 1 is 15.8 atoms g<sup>-1</sup> yr<sup>-1</sup> ( $P_{Qref}$ ). This discrepancy with the calibrated value likely reflects uncertainties in both the excitation functions and the nucleon fluxes considered (Reedy, 2013; Sato et al., 2006; Sato et al., 2008). Giving more credence to the geologically calibrated quartz values, we account for this discrepancy similarly to Lifton et al. (2014), deriving a compositionally dependent site-specific production rate ( $P_{CD}$ ) by normalizing the predicted compositionally dependent production rate at the site of interest ( $P_{CDpred}$ ) by the ratio of  $P_{Qcal}$  to  $P_{Qref}$ , per Eq. 3. Another way to think of this is that the ratio of  $P_{CDpred}$  to  $P_{Qref}$  is the compositionally dependent scaling factor, multiplied by the geologically calibrated production rate in quartz,  $P_{Qcal}$ .

$$P_{CD} = P_{Qcal} \frac{P_{CDpred}}{P_{Qref}} \text{ atoms g}^{-1} \text{ yr}^{-1} \quad (3)$$

We compare  $P_{CD}$  values at SLHL to  $P_{Qcal}$  for compositions reflecting both individual minerals (Barthelmy, 2014) (i.e., mineral separates) and a broad range of silicate rock types (Parker, 1967; Fabryka-Martin, 1988) (i.e., whole-rock analyses) (Table 1). A pure calcite composition (CaCO<sub>3</sub>) is assumed for limestone and MgCa(CO<sub>3</sub>)<sub>2</sub> is assumed for dolomite. Spallation production is only possible from Ca and O, although we included the O number density contribution from CO<sub>2</sub> in the software framework. Thermal neutron production of *in situ* <sup>14</sup>C from <sup>12</sup>C or <sup>13</sup>C is expected to be negligible and is not considered here (e.g., Wright et al., 2019).

## 180 4 Results and Discussion

### 4.1 Predicted modern production rates for silicate minerals and rock types

Predicted SLHL modern (i.e., 2010) spallogenic production rates for *in situ*  $^{14}\text{C}$  in the silicates considered here are generally lower than that from pure quartz (Fig 3; Table 2), but spallation production from O dominates throughout the compositional range we explored (Table 3). As expected from reaction systematics,  $^{14}\text{C}$  production rates tend to decline rapidly with progressively increasing atomic mass of the target nuclide (Fig 3). Interestingly, the production rate predicted for albite using the excitation functions from JENDL/HE-2007 for spallation reactions on  $^{23}\text{Na}$  is comparable to that of quartz. We note that the JENDL/HE-2007 model  $^{23}\text{Na}(\text{n},\text{x})^{14}\text{C}$  excitation function exhibits a broad peak between ca. 30-350 MeV with cross-sections comparable to that of the empirical  $\text{O}(\text{n},\text{x})^{14}\text{C}$  excitation function of Reedy (2013) (Fig. 1), suggesting similar production magnitudes for the two reactions. To our knowledge, no comparable empirical excitation functions for the  $^{23}\text{Na}(\text{n},\text{x})^{14}\text{C}$  or  $^{23}\text{Na}(\text{p},\text{x})^{14}\text{C}$  reactions have been published to date, making the model reactions difficult to validate. Predicted production rates for Mg-rich silicates such as forsterite and enstatite are ca. 7-10% lower than in quartz, while Al-rich minerals such as Ca- and K-feldspars yield production rates 12-13% below quartz. Ca-rich wollastonite exhibits less than 1% of its total  $^{14}\text{C}$  production from Ca, yielding a production rate more than 20% below that of quartz, while Fe-rich minerals such as ferrosilite and fayalite suggest SLHL production rates ca. 32% and 41% less than quartz, respectively. Predicted production rates for two carbonate minerals considered, calcite and dolomite, are 12% and 3% less than quartz, respectively.

The  $P_{\text{CD}}$  values for selected rock types (ultramafic, basalt, high-Ca granite, low-Ca granite, and granodiorite; Fabryka-Martin, 1988) follow a similar pattern to the individual minerals, with total production rates less than that of quartz but with less overall variation (Fig. 3; Table 2). Predicted whole-rock production rates tend to increase with decreasing Fe and Mg content, with  $P_{\text{CD}}$  values ranging from nearly 15% less than quartz for ultramafic compositions to ca. 5-7% below that of quartz for more felsic compositions. As with the idealized mineral compositions, spallation from O dominates *in situ*  $^{14}\text{C}$  production (>90% for all compositions considered), with lesser production from Si, Al, Na, and Mg. Only minor production contributions from Ca and Fe are predicted (typically <1%).

### 4.2 Assessing uncertainty in predicted compositionally dependent production rates

There are three main sources of uncertainty in our predicted production rates, associated with the particle spectra, the geologic production rate calibration for *in situ*  $^{14}\text{C}$  in quartz, and the excitation functions. We note that these are not entirely independent, as the LSDn-based production rate calibration utilizes both the particle spectra of Sato et al. (2008) and excitation functions of Reedy (2013). Sato et al. (2008) quote statistical uncertainties in their modelled particle fluxes on the order of 5-20% between ca. 10 km altitudes and sea level, respectively, although Lifton et al. (2014) note that predictions within this altitude range show good agreement with measured differential fluxes and no evidence of systematic errors. The conservative uncertainty in the recalibrated *in situ*  $^{14}\text{C}$  global production rate in quartz is on the order of 6-7% using the gridded  $R_{\text{C}}$  geomagnetic framework and LSDn scaling. Reedy (2013) suggests uncertainties on the order of 10% for the empirical excitation functions presented. [However, Reedy \(2013\) also suggests that modelled cross-sections may differ from measured ones for a given nuclide by a factor of  \$\approx 2\$ . However](#) Thus, assessing the uncertainty in the modelled functions of JENDL/HE-2007 is more difficult.

We attempted to assess this latter uncertainty by comparing results using JENDL/HE-2007 to predictions incorporating the more recent TENDL-2019 database (Koning et al., 2019). We focused on the proton and neutron excitation functions for  $^{14}\text{C}$



production from  $^{23}\text{Na}$ , since our predictions using the JENDL/HE-2007  $^{23}\text{Na}$  excitation functions suggest comparable production to that from O (Fig. 1; Table 2). However, TENDL-2019 excitation functions only extend to an energy of 200 MeV, although at higher resolution than JENDL/HE-2007. We thus compared albite production rates predicted using the JENDL/HE-2007 excitation function alone ( $\text{Na}_J$ ) with those incorporating spliced neutron and proton excitation functions using TENDL-2019 for  $E \leq 200$  MeV and JENDL/HE-2007 for  $E > 200$  MeV ( $\text{Na}_{TJ}$ ) (Fig. 2).

Neutron and proton excitation functions for  $^{23}\text{Na}$  have similar thresholds of ca. 30-35 MeV in both JENDL/HE-2007 and TENDL-2019 (Fig. 2). Of note, the low-energy peaks in the TENDL-2019 excitation functions are narrower, ca. 30% lower, and occur at a slightly higher energy than those of JENDL/HE-2007 (ca. 150 MeV vs. ca. 90 MeV, respectively). However, the predicted production rate for albite using the spliced  $\text{Na}_{TJ}$  excitation functions is only ca. 3% less than that using the  $\text{Na}_J$  excitation functions alone (Table 2); also reflected in the lower production proportion from Na of ca. 8% in the spliced version, vs. ca. 13% in  $\text{Na}_J$  version (Table 3).

Apart from the modelled  $^{23}\text{Na}$  excitation functions, the remaining modelled excitation functions have only a minor impact on the overall production rates we predict. The percentages of total production of *in situ*  $^{14}\text{C}$  from  $^{55}\text{Mn}$ ,  $^{48}\text{Ti}$ ,  $^{40}\text{Ca}$ ,  $^{39}\text{K}$  and  $^{31}\text{P}$  range from <0.001% to 0.2% for the compositions considered (Table 3). Even if the modelled reaction cross sections are off by a factor of 2, as suggested from Reedy (2013), the impact to overall production is small. For instance, doubling the percentage of  $^{14}\text{C}$  production from Ca for wollastonite would only increase predicted production to 0.4. In addition, we argue that calculating production using modelled excitation functions for only the most abundant isotope of each of these elements, instead of excitation functions reflecting their natural isotopic abundances, introduces negligible additional uncertainty. For example, we assume 100% of production of *in situ*  $^{14}\text{C}$  from  $^{48}\text{Ti}$ , even though  $^{48}\text{Ti}$  comprises only 73% of Ti isotopes. However,  $^{48}\text{Ti}$  contributes <0.001% of total production for the compositions we considered; it is unlikely that including excitation functions for other common Ti isotopes would change that prediction significantly. Similar arguments can be made for the other isotopes referenced above. We therefore argue that the overall additional uncertainty in our predictions that might be introduced by using more conservative estimates of potential errors in the modelled reaction cross sections would be insignificant relative to other uncertainties in the calculations, for the compositions considered. That said, future additional empirical excitation functions for neutron and proton reactions using elements in their natural abundances would likely improve our predictions.

Based on these results, we suggest assuming a 10% uncertainty ~~as well~~ for the JENDL/HE-2007 excitation functions overall, pending empirical validation. Thus, considering the three sources of uncertainty above, we suggest a reasonable estimate of current uncertainty on our theoretical production rates might be on the order of 10-15%, also pending validation with geologic calibrations, assuming extraction and  $\text{CO}_2$  purification hurdles can ultimately be overcome.

### 4.3 Comparisons with previous studies

We compare output of our software framework to two earlier studies that also calculated theoretical *in situ*  $^{14}\text{C}$  production rates from targets of varying composition (Fabryka-Martin, 1988; Masarik, 2002), without adjusting our predictions to the geologically calibrated production rate in quartz. First, Fabryka-Martin (1988) estimated SLHL secular equilibrium *in situ*  $^{14}\text{C}$  concentrations at depths of ~20 cm for ultramafic rock, basalt, high-Ca granite, low-Ca granite, and limestone compositions, following Parker (1967) (Table 4). The equilibrium concentrations were calculated assuming neutron spallation production only from oxygen and a SLHL production rate of 26 atoms  $\text{g}^{-1} \text{yr}^{-1}$  from oxygen (Yokoyama et al., 1977) based on excitation functions from Reedy and Arnold (1972). We derived secular equilibrium SLHL production rates from Fabryka-Martin (1988)

by multiplying the concentrations by the  $^{14}\text{C}$  decay constant of  $1.216 \times 10^{-4} \text{ y}^{-1}$  (Table 4 –  $P_{16\text{O-FM}}$ ). Considering only theoretical production from  $^{16}\text{O}$  in our results (Total  $P_{\text{CDpred}}$  in Table 2 multiplied by the corresponding O production proportion in Table 3), our  $P_{16\text{O}}$  values in Table 4 are ca. 40-45% below those derived from Fabryka-Martin (1988). However, it should be pointed out that Yokoyama et al. (1977) suggest  $\pm 35\%$  uncertainty ( $1\sigma$ ) on their *in situ*  $^{14}\text{C}$  production rate estimate used by Fabryka-Martin (1988), so our theoretical  $P_{16\text{O}}$  values using more accurate particle fluxes and excitation functions lie well within that range.

The second study we considered (Masarik, 2002) is a conference abstract that presents formulas for estimating compositional dependence of *in situ* cosmogenic nuclide SLHL production rates by neutron spallation, including  $^{14}\text{C}$ , derived from numerical simulations. For *in situ*  $^{14}\text{C}$  production, Masarik (2002) considers the target elements O, Mg, Al, Si, and Fe, parameterized in terms of weight fractions of each (Table 5). Total production rates from Masarik (2002) ( $P_{\text{M02}}$ ) in Table 5 are typically ca. 10-20% higher than neutron-only theoretical production rates for rock and mineral compositions considered in this study (Neutron  $P_{\text{CDpred}}$ , Table 2). Being an abstract, details underlying the simulations and calculations in Masarik (2002) are sparse, but we suggest a combination of differences in the differential neutron flux spectra (Masarik and Beer, 1999, vs. Sato et al., 2008) and excitation functions (e.g., Reedy and Masarik, 1995, vs. Reedy, 2013) used in the two studies, as well as unstated uncertainties in the Masarik (2002) coefficients, may be the sources of the discrepancies in the predictions of the respective studies.

[We derived a similar elemental parameterization to that of Masarik \(2002\) for SLHL \*in situ\*  \$^{14}\text{C}\$  production as part of this study, but including production from both neutrons and protons for all of the elements we consider, given by](#)

$$\begin{aligned} P_{\text{CDpred}} = & 29.01[\text{O}] + 15.59[\text{Na}] + 2.19[\text{Mg}] + 1.67[\text{Al}] + 0.84[\text{Si}] + 0.22[\text{P}] \\ & + 0.10[\text{Fe}] + 0.08[\text{K}] + 0.06[\text{Ca}] + 0.05[\text{Ti}] + 0.03[\text{Mn}] \end{aligned} \quad (4)$$

[where the bracketed values are the respective elemental fractions derived from the measured major elemental analysis. \*In situ\*  \$^{14}\text{C}\$  production rates predicted using this equation for the compositions considered Table 1 are identical to the  \$P\_{\text{CDpred}}\$  values in Table 2, since both are derived using the same software framework.](#)

In addition to the theoretical studies, Handwerger et al. (1999) measured *in situ*  $^{14}\text{C}$  concentrations in carbonate deposits (limestone bedrock and tufa) from well-preserved Provo-level shoreline features associated with Pleistocene Lake Bonneville, Utah, to calibrate *in situ*  $^{14}\text{C}$  spallogenic production rates in calcite. The late Pleistocene lake-level history of Lake Bonneville is well-constrained by traditional radiocarbon dates and has been used for geological calibration of a number of cosmogenic nuclides (Lifton et al., 2015a). *In situ*  $^{14}\text{C}$  measurements in Handwerger et al. (1999) were reduced according to standard methods for radiocarbon in organic materials, but Hippe and Lifton (2014) subsequently developed comprehensive data reduction procedures specifically for *in situ*  $^{14}\text{C}$ . Unfortunately, Handwerger et al. (1999) do not present full details of their analytical results and calculations – we thus cannot correct their data to current standards using the Hippe and Lifton (2014) protocols. If we assume such corrections would be small relative to the resulting *in situ*  $^{14}\text{C}$  concentrations in their calibration samples, neglecting three anomalous results, and using the age of initial Provo shoreline formation from Lifton et al. (2015a) of  $18.3 \pm 0.3 \text{ ka BP}$ , their mean *in situ*  $^{14}\text{C}$  concentration is  $(3.75 \pm 0.26) \times 10^5 \text{ atoms g}^{-1} \text{ CaCO}_3$ . This corresponds to a local production rate of ca.  $51 \text{ atoms g}^{-1} \text{ yr}^{-1}$ . In contrast, the theoretical local production rate calculated with our software framework is ca.  $43.9 \text{ atoms g}^{-1} \text{ yr}^{-1}$ ,  $\sim 15\%$  lower than the derived local production rate. In addition, the predicted value normalized to  $P_{\text{Qcal}}$  yields  $37.5 \text{ atoms g}^{-1} \text{ yr}^{-1}$ ,  $27\%$  lower than Handwerger et al. (1999). Given the uncertainties in the uncorrected Handwerger et



290 al. (1999) dataset, and the suggested uncertainties in our method, we find reasonable agreement between our production rate estimates and that of Handwerger et al. (1999).

## 5 Conclusions

As a first step in exploring potential applications of *in situ*  $^{14}\text{C}$  to quartz-poor or fine-grained rock types, we have extended the functionality of the MATLAB®-based LSDn nuclide-specific scaling framework (Lifton et al., 2014; Lifton, 2016) to  
295 estimate spallogenic production of *in situ*  $^{14}\text{C}$  in rock and mineral compositions other than pure quartz at sites of interest. We account for compositionally dependent production by using measured and modelled nucleon excitation functions for target elements in major element oxide analyses (e.g., XRF), in concert with secondary cosmic-ray differential fluxes per Lifton et al. (2014). The ratio of resulting theoretical compositionally dependent *in situ*  $^{14}\text{C}$  production rates to the corresponding theoretical quartz production rate are then multiplied by the geologically calibrated production rate in quartz, placing the theoretical  
300 production rates in a calibrated context. Exploring a broad range of mineral and rock compositions indicates production is dominated by oxygen spallation as expected (>90% at SLHL), but with a general decrease in total production rate with more mafic (particularly Fe-rich) compositions. Although this study confirms previous work identifying Si, Mg, and Al as important targets, we also find for the first time that Na appears to contribute significantly. Future nucleon excitation function measurements, particularly for Na reactions, should improve the robustness of this software tool further. This framework is thus  
305 an important initial step forward in applying *in situ*  $^{14}\text{C}$  to a broader array of landscapes.

## Code availability

The MATLAB® scripts referenced in this manuscript are available at <https://github.com/nlifton/CD14C>. A permanent DOI will be provided upon acceptance of this manuscript.

## Author contributions

310 The study was conceived by NL and AK. AK and NL developed the MATLAB® scripts. Manuscript was written by AK and NL.

## Competing interests

The authors declare no competing interests.

## Acknowledgements

NL received support from the U.S. National Science Foundation (NSF) award EAR-1560658. AK acknowledges support from a  
315 Purdue Research Foundation Ross Fellowship/Assistantship.

## References

Balco, G., Stone, J. O., Lifton, N. A. and Dunai, T. J.: A complete and easily accessible means of calculating surface exposure ages or erosion rates from  $^{10}\text{Be}$  and  $^{26}\text{Al}$  measurements, *Quat. Geochron.*, 3(3), 174–195, doi:10.1016/j.quageo.2007.12.001, 2008.

- Barthelmy, D., Mineralogy Database, <http://www.webmineral.com>, 2014, accessed July 8, 2020
- Bevington P. R. and Robinson D. K., Data Reduction and Error Analysis for the Physical Sciences. McGraw-Hill, New York, N.Y., 1992
- Borchers, B., Marrero, S., Balco, G., Caffee, M., Goehring, B., Lifton, N., Nishiizumi, K., Phillips, F., Schaefer, J. and Stone, J.: Geological calibration of spallation production rates in the CRONUS-Earth project, *Quat. Geochron.*, 31, 188–198, doi:10.1016/j.quageo.2015.01.009, 2016.
- Brown, D. A., Chadwick, M. B., Capote, R., Kahler, A. C., Trkov, A., Herman, M. W., Sonzogni, A. A., Danon, Y., Carlson, A. D., Dunn, M., Smith, D. L., Hale, G. M., Arbanas, G., Arcilla, R., Bates, C. R., Beck, B., Becker, B., Brown, F., Casperson, R. J., Conlin, J., Cullen, D. E., Descalle, M. A., Firestone, R., Gaines, T., Guber, K. H., Hawari, A. I., Holmes, J., Johnson, T. D., Kawano, T., Kiedrowski, B. C., Koning, A. J., Kopecky, S., Leal, L., Lestone, J. P., Lubitz, C., Márquez Damián, J. I., Mattoon, C. M., McCutchan, E. A., Mughabghab, S., Navratil, P., Neudecker, D., Nobre, G. P. A., Noguere, G., Paris, M., Pigni, M. T., Plompen, A. J., Pritychenko, B., Pronyaev, V. G., Roubtsov, D., Rochman, D., Romano, P., Schillebeeckx, P., Simakov, S., Sin, M., Sirakov, I., Sleaford, B., Sobes, V., Soukhovitskii, E. S., Stetcu, I., Talou, P., Thompson, I., van der Marck, S., Welser-Sherrill, L., Wiarda, D., White, M., Wormald, J. L., Wright, R. Q., Zerkle, M., Žerovnik, G. and Zhu, Y.: ENDF/B-VIII.0: The 8<sup>th</sup> Major Release of the Nuclear Reaction Data Library with CIELO-project Cross-sections, New Standards and Thermal Scattering Data, *Nucl. Data Sheets*, 148, 1–142, doi:10.1016/j.nds.2018.02.001, 2018.
- Brown, E. T., Trull, T. W., Jean-baptiste, P., Raisbeck, G., Bourles, D., Yiou, F. and Marty, B.: Determination of cosmogenic production rates of  $^{10}\text{Be}$ ,  $^3\text{He}$  and  $^3\text{H}$  in water, *Nucl. Instruments Methods Phys. Res. B*, 172, 873–883, 2000.
- Chmeleff, J., von Blanckenburg, F., Kossert, K. and Jakob, D.: Determination of the  $^{10}\text{Be}$  half-life by multicollector ICP-MS and liquid scintillation counting, *Nucl. Inst. Methods Phys. Res. B*, 268(2), 192–199, doi:10.1016/j.nimb.2009.09.012, 2010.
- Cooke, D. J., Humble, J. E., Shea, M. A., Smart, D. F., Lund, N., Rasmussen, I. L., Byrnak, B., Goret, P. and Petrou, N.: On cosmic-ray cut-off terminology, *Nuovo Cim. C*, 14(3), 213–234, doi:10.1007/BF02509357, 1991.
- Fabryka-Martin, J. T.: Production of radionuclides in the earth and their hydrogeologic significance, with emphasis on chlorine-36 and iodine-129. Ph.D. thesis, The University of Arizona., 1988.
- Fukahori, T., Watanabe, Y., Yoshizawa, N., Maekawa, F., Meigo, S. I., Konno, C., Yamano, N., Konobeyev, A. Y. and Chiba, S.: JENDL high energy file, *J. Nucl. Sci. Technol.*, 39, 25–30, doi:10.1080/00223131.2002.10875031, 2002.
- Fülöp, R. H., Fink, D., Yang, B., Codolean, A. T., Smith, A., Wacker, L., Levchenko, V. and Dunai, T. J.: The ANSTO – University of Wollongong in-situ  $^{14}\text{C}$  extraction laboratory, *Nucl. Instruments Methods Phys. Res. Sect. B Beam Interact. With Mater. Atoms*, 438(January 2018), 207–213, doi:10.1016/j.nimb.2018.04.018, 2019.
- Goehring, B. M., Wilson, J. and Nichols, K.: A fully automated system for the extraction of *in situ* cosmogenic carbon-14 in the Tulane University cosmogenic nuclide laboratory, *Nucl. Instruments Methods Phys. Res. Sect. B Beam Interact. With Mater. Atoms*, (December 2017), 1–9, doi:10.1016/j.nimb.2019.02.006, 2019.
- Gosse, J. C. and Phillips, F. M.: Terrestrial *in situ* cosmogenic nuclides: theory and application, *Quat. Sci. Rev.*, 20, 1475–1560, doi:10.1016/S0277-3791(00)00171-2, 2001.
- Grieder, P., *Cosmic Rays at Earth: Researcher's Reference Manual and Data Book*, 1<sup>st</sup> ed. Elsevier, Amsterdam, 2001.
- Handwerger, D. A., Cerling, T. E. and Bruhn, R. L.: Cosmogenic  $^{14}\text{C}$  in carbonate rocks, *Geomorphology*, 27(March 1998), 1999.
- Heisinger, B., Lal, D., Jull, a. J. T., Kubik, P., Ivy-Ochs, S., Neumaier, S. and Knie, K., Lazarev, V. and Nolte, E.: Production of selected cosmogenic radionuclides by muons 1. Fast muons, *Earth Planet. Sci. Lett.*, 200(3–4), 345–355, doi:10.1016/S0012-821X(02)00640-4, 2002a.
- Heisinger, B., Lal, D., Jull, A. J. T., Kubik, P., Ivy-Ochs, S., Knie, K. and Nolte, E.: Production of selected cosmogenic radionuclides by muons: 2. Capture of negative muons, *Earth Planet. Sci. Lett.*, 200(3–4), 357–369, doi:10.1016/S0012-821X(02)00641-6, 2002b.
- Hippe, K., Jansen, J. D., Skov, D. S., Lupker, M., Ivy-Ochs, S., Kober, F., Zeilinger, G., Capriles, J. M., Christl, M., Maden, C., Vockenhuber, C. and Egholm, D. L.: Cosmogenic *in situ*  $^{14}\text{C}$ - $^{10}\text{Be}$  reveals abrupt Late Holocene soil loss in the Andean Altiplano, *Nat. Commun.*, 12, 1–9, doi:10.1038/s41467-021-22825-6, 2021.
- Hippe, K.: Constraining processes of landscape change with combined *in situ* cosmogenic  $^{14}\text{C}$ - $^{10}\text{Be}$  analysis, *Quat. Sci. Rev.*, 173, 1–19, doi:10.1016/j.quascirev.2017.07.020, 2017.

- Hippe, K., Kober, F., Wacker, L., Fahrni, S. M., Ivy-Ochs, S., Akçar, N., Schlüchter, C. and Wieler, R.: An update on *in situ* cosmogenic  $^{14}\text{C}$  analysis at ETH Zürich, Nucl. Instruments Methods Phys. Res. Sect. B Beam Interact. With Mater. Atoms, 294, 81–86, doi:10.1016/j.nimb.2012.06.020, 2013.
- Hippe, K. and Lifton, N. A. Calculating isotope ratios and nuclide concentrations for *in situ* cosmogenic  $^{14}\text{C}$  analyses. Radiocarb., 56(3), 1167–1174. <https://doi.org/10.2458/56.17917>, 2014.
- Imamura, M., Nagai, H., Takabatake, M., Shibata, S., Kobayashi, K., Yoshida, K., Ohashi, H., Uwamino, Y. and Nakamura, T.: Measurements of production cross sections of C and  $^{26}\text{Al}$  with high-energy neutrons up to  $E_n = 38$  MeV by accelerator mass spectrometry, Nucl. Inst. Methods Phys. Res. B, 52(3–4), 595–600, doi:10.1016/0168-583X(90)90482-A, 1990.
- Jull, A. J. T., Cloutd, S., Donahue, D. J., Sisterson, J. M., Reedy, R. C. and Masarik, J.:  $^{14}\text{C}$  depth profiles in Apollo 15 and 17 cores and lunar rock 68815, Geochim. Cosmochim. Acta, 62(17), 3025–3036, doi:10.1016/S0016-7037(98)00193-8, 1998.
- Jull, A. J. T., Lifton, N., Phillips, W., & Quade, J., Studies of the production rate of cosmic-ray produced  $^{14}\text{C}$  in rock surfaces. Nucl. Inst. Methods Phys. Res. B 92, 308–310, 1994.
- Jull, A.T.J., Wilson, A.E., Donahue, D.J., Toolin, L.J., Burr, G.S., Measurements of cosmogenic  $^{14}\text{C}$  produced by spallation in high- altitude rocks. Radiocarbon 34, 737-744, 1992.
- Jull, A. J. T., Donahue, D. J. and Linick, T. W.: Carbon-14 activities in recently fallen meteorites and Antarctic meteorites, Geochim. Cosmochim. Acta, 53(8), 2095–2100, doi:10.1016/0016-7037(89)90327-X, 1989.
- Koning, A. J., Rochman, D., Sublet, J., Dzysiuk, N., Fleming, M. and Marek, S. Van Der: TENDL : Complete Nuclear Data Library for Innovative Nuclear Science and Technology, Nucl. Data Sheets, 155, 1–55, doi:10.1016/j.nds.2019.01.002, 2019.
- Korschinek, G., Bergmaier, A., Faestermann, T., Gerstmann, U. C., Knie, K., Rugel, G., Wallner, A., Dillmann, I., Dollinger, G., Lierse von Gostomski, C., Kossert, K., Maiti, M., Poutivtsev, M. and Remmert, A.: A new value for the half-life of  $^{10}\text{Be}$  by Heavy-Ion Elastic Recoil Detection and liquid scintillation counting, Nucl. Inst. Methods Phys. Res. B, 268(2), 187–191, doi:10.1016/j.nimb.2009.09.020, 2010.
- Lifton, N., Caffee, M., Finkel, R., Marrero, S., Nishiizumi, K., Phillips, F.M., Goehring, B., Gosse, J., Stone, J., Schaefer, J., Theriault, B., Jull, A.J.T., Fifield, K., ~~in-situ~~*in situ* cosmogenic nuclide production rate calibration for the CRONUS-Earth project from Lake Bonneville, Utah, shoreline features. Quat. Geochron. 26, 55-69. Doi:10.1016/j.quageo.2014.11.002, 2015a.
- Lifton, N., Goehring, B., Wilson, J., Kubley, T. and Caffee, M.: Progress in automated extraction and purification of *in situ*  $^{14}\text{C}$  from quartz: Results from the Purdue *in situ*  $^{14}\text{C}$  laboratory, Nucl. Instruments Methods Phys. Res. Sect. B Beam Interact. With Mater. Atoms, 361, 381–386, doi:10.1016/j.nimb.2015.03.028, 2015b.
- Lifton, N., Sato, T. and Dunai, T. J.: Scaling *in situ* cosmogenic nuclide production rates using analytical approximations to atmospheric cosmic-ray fluxes, Earth Planet. Sci. Lett., 386, 149–160, doi:10.1016/j.epsl.2013.10.052, 2014.
- Lifton, N. A., Smart, D. F. and Shea, M. A.: Scaling time-integrated *in situ* cosmogenic nuclide production rates using a continuous geomagnetic model, Earth Planet. Sci. Lett., 268, 190–201, doi:10.1016/j.epsl.2008.01.021, 2008.
- Lifton, N., Jull, A. J. T. and Quade, J.: A new extraction technique and production rate estimate for *in situ* cosmogenic  $^{14}\text{C}$  in quartz, Geochim. Cosmochim. Acta, 65(12), 1953–1969, doi:10.1016/S0016-7037(01)00566-X, 2001.
- Lifton N. A. (1997) A new extraction technique and production rate estimate for ~~in-situ~~*in situ* cosmogenic  $^{14}\text{C}$  in quartz. Ph.D. Dissertation, University of Arizona.
- Lupker, M., Hippe, K., Wacker, L., Steinemann, O., Tikhomirov, D., Maden, C., Haghipour, N. and Synal, H. A.: In-situ cosmogenic  $^{14}\text{C}$  analysis at ETH Zürich: Characterization and performance of a new extraction system, Nucl. Instruments Methods Phys. Res. Sect. B Beam Interact. With Mater. Atoms, 457(March), 30–36, doi:10.1016/j.nimb.2019.07.028, 2019.
- Lupker, M., Hippe, K., Wacker, L., Kober, F., Maden, C., Braucher, R., Bourlès, D., Romani, J. R. V. and Wieler, R.: Depth-dependence of the production rate of *in situ*  $^{14}\text{C}$  in quartz from the Leymon High core, Spain, Quat. Geochron., 28, 80–87, doi:10.1016/j.quageo.2015.04.004, 2015.
- Marrero, S.M., Phillips, F.M., Caffee, M.W., and Gosse, J.C., CRONUS-Earth cosmogenic  $^{36}\text{Cl}$  calibration: Quat. Geochron. 31, 199–219, doi:10.1016/j.quageo.2015.10.002, 2016a.
- Marrero, S. M., Phillips, F. M., Borchers, B., Lifton, N., Aumer, R. and Balco, G.: Cosmogenic nuclide systematics and the CRONUScalc program, Quat. Geochron., 31, 160–187, doi:10.1016/j.quageo.2015.09.005, 2016b.

- Masarik, J. and Beer, J.: An updated simulation of particle fluxes and cosmogenic nuclide production in the Earth's atmosphere, *J. Geophys. Res.*, 114, 1–9, doi:10.1029/2008JD010557, 2009.
- 420 Masarik, J., Numerical simulation of in-situ production of cosmogenic nuclides, *Geochim. Cosmochim. Acta* 66, Suppl. 1, A491, 2002.
- Masarik, J. and Reedy, R. C.: Monte Carlo simulations of in-situ-produced cosmogenic nuclides, in *Santa Fe Workshop on Secular Variations*, 163–164., 1995.
- Martin, L. C. P., Blard, P. H., Balco, G., Lavé, J., Delunel, R., Lifton, N. and Laurent, V.: The CREP program and the ICE-D production rate calibration database: A fully parameterizable and updated online tool to compute cosmic-ray exposure ages, 425 *Quat. Geochron.*, 38, 25–49, doi:10.1016/j.quageo.2016.11.006, 2017.
- Michel, R., Gloris, M., Lange, H.-J., Leya, I., Lupke, M., Herpers, U., Dittrich-Hannen, B., Rosel, R., Schiek, T., Filges, D., Dragovitsch, P., Sutter, M., Hofmann, H.-J., Wolfi, W., Kubik, P. W., Baur, H. and Wieler, R.: Nuclide production by proton-induced reactions on elements ( $6 < Z < 29$ ) in the energy range from 800 to 2600 MeV, *Nucl. Instr. Methods Phys. Res. B*, 103, 183–222, 1995.
- 430 Nishiizumi, K., Preparation of  $^{26}\text{Al}$  AMS standards. *Nuclear. Instr. Meth. Phys. Res. B*, 223, 388–392, doi:10.1016/j.nimb.2004.04.075, 2004.
- Nishiizumi, K., Finkel, R.C., Klein, J., Kohl, C.P., Cosmogenic production of  $^7\text{Be}$  and  $^{10}\text{Be}$  in water targets. *Journal of Geophysical Research* 101, 22,225–22,232, 1996.
- Parker, R. L., Data of Geochemistry, U. S. Geol. Surv. Prof. Paper 440-D, ed. M. Fleischer, 19 p., 1967.
- 435 Pavón-Carrasco, F.J., Osete, M.L., Torta, J.M., De Santis, A., A geomagnetic field model for the Holocene based on archaeomagnetic and lava flow data. *Earth Planet. Sci. Lett.* 388, 98–109, 2014.
- Reedy, R. C.: Cosmogenic-nuclide production rates: Reaction cross section update, *Nucl. Instr. Meth. Phys. Res. B*, 294, 470–474, doi:10.1016/j.nimb.2011.08.034, 2013.
- Reedy, R. C.: Proton cross-sections for producing cosmogenic radionuclides, *Lunar Planet. Sci* 38, 1329–1330, 2007.
- 440 Reedy, R.C., A model for GCR-particle fluxes in stony meteorites and production rates of cosmogenic nuclides: *Journal of Geophys. Res.* 90, Suppl., C722–C728, doi:10.1029/jb090is02p0c722, 1985.
- Sato, T. and Niita, K.: Analytical functions to predict cosmic-ray neutron spectra in the atmosphere, *Radiat. Res.*, 166(3), 544–555, doi:10.1667/RR0610.1, 2006.
- 445 Sato, T., Yasuda, H., Niita, K., Endo, A., Sihver, L., Sato, T., Yasuda, H., Niita, K., Endo, A. and Sihver, L.: Development of PARMA: PHITS-Based Analytical Radiation Model in the Atmosphere, *Radiat. Res.*, 170(2), 244–259, 2008.
- Schimmelpfennig, I., Schaefer, J. M., Goehring, B. M., Lifton, N., Putnam, A. E. and Barrell, D. J. A.: Calibration of the *in situ* cosmogenic  $^{14}\text{C}$  production rate in New Zealand's Southern Alps, *J. Quat. Sci.*, 27, 671–674, doi:10.1002/jqs.2566, 2012.
- 450 Sisterson, J. M., Schneider, R. J. I., Jull, A. J. T., Donahue, D. J., Cloudt, S., Kim, K., Beverding, A., Englert, P. A. J., Castaneda, C., Vincent, J. and Reedy, R. C.: Revised solar cosmic ray fluxes estimated using measured depth profiles of  $^{14}\text{C}$  in Lunar rocks; The importance of good  $^{14}\text{C}$  cross section determinations, *Lunar Planet. Sci.* 22, 1996.
- Sisterson, J., Jull, A. J. T., Beverding, A., Koehler, A. M., Castaneda, C., Vincent, J., Donahue, D. J., Englert, P. A. J., Gans, C., Young, J. and Reedy, R. C.: Proton production cross-sections for  $^{14}\text{C}$  from silicon and oxygen: implications for cosmic-ray studies, *Nucl. Instruments Methods Phys. Res. B*, 92, 510–512, 1994.
- Thomas, J. H., Rau, R. L., Skelton, R. T. and Kavanagh, R. W.: Half-life of  $^{26}\text{Al}$ , *Phys. Rev. C*, 30(1), 385–387, 1984.
- 455 Vermeesch, P., Baur, H., Heber, V. S., Kober, F., Oberholzer, P., Schaefer, J. M., Schlüchter, C., Strasky, S. and Wieler, R.: Cosmogenic  $^3\text{He}$  and  $^{21}\text{Ne}$  measured in targets after one year of exposure in the Swiss Alps, *Earth Planet. Sci. Lett.*, 284(3–4), 417–425, doi:10.1016/j.epsl.2009.05.007, 2009.
- Von Blanckenburg, F.: The control mechanisms of erosion and weathering at basin scale from cosmogenic nuclides in river sediment, *Earth Planet. Sci. Lett.*, 237(3–4), 462–479, doi:10.1016/j.epsl.2005.06.030, 2005.
- 460 Watanabe, Y., Kosako, K., Kunieda, S., Chiba, S., Fujimoto, R., Harada, H., Kawai, M., Maekawa, F., Murata, T., Nakashima, H., Niita, K., Shigyo, N., Shimakawa, S., Yamano, N. and Fukahori, T.: Status of JENDL high energy file, *J. Korean Phys. Soc.*, 59(23), 1040–1045, doi:10.3938/jkps.59.1040, 2011.

- 465 Wright, T., Bennett, S., Heinitz, S., Köster, U., Mills, R., Soldner, T., Steier, P., Wallner, A., and Wieninger, T., Measurement of the  $^{13}\text{C}(\text{n},\gamma)$  thermal cross section via neutron irradiation and AMS, Eur. Phys. J. A, 55, 200, doi:10.1140/epja/i2019-12893-0, 2019.
- Yokoyama, Y., Reyss, J. L. and Guichard, F.: Production of radionuclides by cosmic rays at mountain altitudes, Earth Planet. Sci. Lett., 36(1), 44–50, doi:10.1016/0012-821X(77)90186-8, 1977.
- 470 Young, N. E., Schaefer, J. M., Goehring, B., Lifton, N., Schimmelpfennig, I. and Briner, J. P.: West Greenland and global *in situ*  $^{14}\text{C}$  production-rate calibrations, J. Quat. Sci., 29(5), 401–406, doi:10.1002/jqs.2717, 2014.

## Figures

**Figure 1:** Measured (Reedy, 2013) (top panels) and modelled (bottom panels) neutron and proton reaction excitation functions for *in situ*  $^{14}\text{C}$  production from various targets. The lines represent the linearly interpolated between points. Note that modelled predictions for  $^{23}\text{Na}$  (JENDL/HE-2007; Fukahorita et al., 2002; Watanabe et al., 2011) suggest the highest production of all nuclides considered.

**Figure 2:** Modelled neutron (top) and proton (bottom) cross-sections for  $^{23}\text{Na}$  from JENDL/HE-2007 ( $\text{Na}_J$ , solid line) compared to the spliced TENDL-2019 at energies  $\leq 0.2$  GeV and JENDL/HE-2007  $> 0.2$  GeV ( $^{23}\text{Na}_{TJ}$ , dashed line). Differential neutron and proton fluxes at SLHL (Sato et al., 2008) are plotted in their respective panes to illustrate the combined effect of excitation function and flux on *in situ*  $^{14}\text{C}$  production.

**Figure 3:** Predicted SLHL production of *in situ*  $^{14}\text{C}$  in minerals (left) and rocks (right) compared relative to that in pure quartz (dashed grey line). The color of each mineral and rock symbol reflects for what the element that contributes the highest proportion of production after oxygen and silica.

## Tables

**Table 1:** Elemental oxide compositions (weight %) for selected silicate minerals (Barthelmy, 2014) and rock types (Parker, 1967), used to calculate number densities (Eq. 2).

**Table 2:** Predicted modern *in situ*  $^{14}\text{C}$  spallogenic production rates (atoms  $\text{g}^{-1} \text{y}^{-1}$ ) at SLHL from neutrons and protons in minerals and rock types considered, both theoretical ( $P_{\text{CDpred}}$ ) and normalized to calibrated production in quartz ( $P_{\text{CD}}$ ) using the gridded  $R_C$  record of Lifton (2016).

**Table 3:** Percentage of total predicted modern *in situ*  $^{14}\text{C}$  production at SLHL by element for each mineral and rock type considered

**Table 4:** Predicted modern *in situ*  $^{14}\text{C}$  production rates at SLHL for neutron spallation from  $^{16}\text{O}$  derived from secular equilibrium concentrations ( $N_{SE}$ ) at ca. 20-cm depth for different rock types (Fabryka-Martin, 1988) compared to our software framework. Note that these estimates are not normalized relative to  $P_{Qcal}$ , for straightforward comparison to Fabryka-Martin's (1988) predictions.

**Table 5:** Neutron-only SLHL *in situ*  $^{14}\text{C}$  production based on Masarik (2002;  $P_{M02}$ ) theoretical predictions for compositions considered in this work, compared to modern SLHL neutron-only production predicted here (also see Table 2). Note that these estimates are not normalized relative to  $P_{Qcal}$ , to enable direct comparison to Masarik's (2002) predictions.



**Table 1:**

Mineral	Composition	SiO <sub>2</sub>	TiO <sub>2</sub>	Al <sub>2</sub> O <sub>3</sub>	FeO	Fe <sub>2</sub> O <sub>3</sub>	MnO	MgO	CaO	Na <sub>2</sub> O	K <sub>2</sub> O	P <sub>2</sub> O <sub>5</sub>	LOI <sup>2</sup>
Quartz	SiO <sub>2</sub>	100	-	-	-	-	-	-	-	=	=	=	=
Albite	NaAlSi <sub>3</sub> O <sub>8</sub>	68.745 2.37	-	19.442 9.62	-	-	-	-	-	11.8218.01	=	=	=
Anorthite	CaAl <sub>2</sub> Si <sub>2</sub> O <sub>8</sub>	43.19	-	36.64	-	-	-	-	20.16	=	=	=	=
Orthoclase	KAlSi <sub>3</sub> O <sub>8</sub>	64.76	-	18.32	-	-	-	-	-	=	16.92	=	=
Forsterite	Mg <sub>2</sub> SiO <sub>4</sub>	42.71	-	-	-	-	-	57.30	-	=	=	=	=
Fayalite	Fe <sub>2</sub> SiO <sub>4</sub>	29.49	-	-	70.51	-	-	-	-	=	=	=	=
Wollastonite	Ca <sub>2</sub> Si <sub>2</sub> O <sub>6</sub>	51.72	-	-	-	-	-	-	48.28	=	=	=	=
Augite <sup>1</sup>	(Ca,Mg,Fe)(Mg,Fe)Si <sub>2</sub> O <sub>6</sub> (Ca,Na)(Mg,Fe, Al,Ti)(Si,Al) <sub>2</sub> O <sub>6</sub>	24.184 8.30	-3.38	-8.63	16.836 08	-	-	7.3215 35	10.352 1.35	-1.31	=	=	=
Ferrosilite	Fe <sub>2</sub> Si <sub>2</sub> O <sub>6</sub>	45.54	-	-	54.46	-	-	-	-	=	=	=	=
Enstatite	Mg <sub>2</sub> Si <sub>2</sub> O <sub>6</sub>	59.85	-	-	-	-	-	40.15	-	=	=	=	=
Calcite <sup>2</sup>	CaCO <sub>3</sub>	-	-	-	-	-	-	-	56.03	=	=	=	43.97
Dolomite <sup>2</sup>	CaMg(CO <sub>3</sub> ) <sub>2</sub>	-	-	-	-	-	-	21.86	30.41	=	=	=	47.73
<b>Rock type<sup>3</sup></b>													
Ultramafic	—	40.64	0.05	0.66	-	14.09	0.19	42.94	0.98	0.77	0.04	0.04	=
Basalt	—	51.34	1.50	16.55	-	12.24	0.26	7.46	9.40	2.62	1.00	0.32	=
Hi-Ca Granite	—	67.16	0.57	15.49	-	4.23	0.07	1.56	3.54	3.83	3.04	0.21	=
Low-Ca Granite	—	74.22	0.20	13.60	-	2.03	0.05	0.27	0.71	3.48	5.06	0.14	=
Granodiorite	—	69.09	0.57	14.55	-	3.86	0.08	0.93	2.21	3.73	4.02	0.16	=

<sup>1</sup> Assumed empirical composition of augite (Morimoto, 1988; <https://www.mindat.org/min-419.html>): (Ca<sub>0.6</sub>Mg<sub>0.2</sub>Fe<sub>0.2</sub>)(Mg<sub>0.5</sub>Fe<sub>0.5</sub>)Si<sub>2</sub>O<sub>6</sub>(Barthelmy, 2014): (Ca<sub>0.9</sub>Na<sub>0.1</sub>)(Mg<sub>0.9</sub>Fe<sub>0.1</sub>Al<sub>0.2</sub>Ti<sub>0.1</sub>)Si<sub>1.9</sub>O<sub>6</sub>

515 <sup>2</sup> LOI = Loss on ignition. [Used in oxygen number density calculation for carbonates; Assumed-assumed](#) to be entirely CO<sub>2</sub>- [in those cases for carbonates, u\\_ sed in oxygen number density calculation](#)

<sup>3</sup> Compositions from Parker (1967)

520 Table 2

<b>Mineral</b>	<i>Neutron <math>P_{CDpred}</math></i> <i>at g<sup>-1</sup> y<sup>-1</sup></i>	<i>Proton <math>P_{CDpred}</math></i> <i>at g<sup>-1</sup> y<sup>-1</sup></i>	<i>Total <math>P_{CDpred}</math></i> <i>at g<sup>-1</sup> y<sup>-1</sup></i>	<i><math>P_{CD}</math></i> <i>at g<sup>-1</sup> y<sup>-1</sup></i>	<i>% Diff <math>P_{CD}</math> vs. <math>P_{Qcal}</math></i>
<i>Quartz</i>	15.37	0.47	15.84	13.5350	0.0
<i>Albite</i>	15.4955	0.48	15.97604	13.6170	0.812
<i>Albite<sup>1</sup></i>	14.9574	0.48	15.4322	13.1500	-42.60
<i>Anorthite</i>	13.43	0.42	13.85	11.80	-12.6
<i>Orthoclase</i>	13.2035	0.3942	13.6077	11.5973	-14.231
<i>Forsterite</i>	13.676	0.46	14.12	12.03	-10.9
<i>Fayalite</i>	9.017	0.278	9.35	7.917	-41.40
<i>Wollastonite</i>	11.85	0.36	12.21	10.41	-22.9
<i>Augite</i>	12.00328	0.3742	12.38370	10.54167	-21.9136
<i>Ferrosilite</i>	10.46	0.32	10.78	9.18	-32.0
<i>Enstatite</i>	14.187	0.46	14.64	12.4750	-7.6
<i>Calcite</i>	13.55	0.38	13.943	11.887	-12.04
<i>Dolomite</i>	14.96	0.44	15.404	13.123	-2.8
<b>Rock</b>					
<i>Ultramafic</i>	13.11	0.43	13.54	11.56	-14.5
<i>Basalt</i>	13.72	0.43	14.15	12.08	-10.7
<i>Hi-Ca Granite</i>	14.30	0.44	14.75	12.59	-6.9
<i>Low-Ca Granite</i>	14.52	0.45	14.97	12.79	-5.5
<i>Granodiorite</i>	14.27	0.44	14.71	12.57	-7.1

<sup>1</sup>Production is calculated using the spliced TENDL-2019 and JENDL/HE-2007 proton and neutron excitation functions (Na<sub>TJ</sub> in text). [All other Na production rates use JENDL/HE-2007 exclusively.](#)

525

**Table 3**

	O	Si	Ti	Al	Fe <sup>2+</sup>	Fe <sup>3+</sup>	Mn	Mg	Ca	Na	K	P
<b>Minerals</b>												
<i>Quartz</i>	97.5	2.5	-	-	-	-	-	-	-	-	-	-
<i>Albite</i>	88.67 09	1.702 9	-	1.086 3	-	-	-	-	-	8.564 2.99	-	-
<i>Albite<sup>1</sup></i>	88.62	1.36	-	1.72	-	-	-	-	-	8.30	-	-
<i>Anorthite</i>	96.37	1.23	-	2.33	-	-	-	-	0.07	-	<0.01	-
<i>Orthoclase</i>	98.11 6.89	0.634 85	-	1.197	-	-	-	-	-	-	0.08	-
<i>Forsterite</i>	93.45 4	1.19	-	-	-	-	-	5.367	-	-	-	-
<i>Fayalite</i>	98.14	1.254	-	-	0.61-	-0.64	-	-	-	-	-	-
<i>Wollastonite</i>	98.16	1.67	-	-	--	--	-	-	0.178	-	-	-
<i>Augite</i>	96.87 5.35	1.653 9	- <0.01	-0.56	<0.01 -	- <0.01	-	1.304 8	0.075	1.11	-	-
<i>Ferrosilite</i>	97.93	1.66	-	-	0.41-	-0.41	-	-	-	-	-	-
<i>Enstatite</i>	94.77 6	1.61	-	-	-	--	-	3.623	-	-	-	-
<i>Calcite</i>	99.82	-	-	-	-	--	-	-	0.18	-	-	-
<i>Dolomite</i>	98.04 49	-	-	-	-	-	-	1.877 4	0.097	-	-	-
<b>Rock type</b>												
<i>Ultramafic</i>	93.84	1.18	<0.01	0.04	<0.01 0.08	0.08< 0.04	<0.01	4.20	<0.01	0.66	<0.01	<0.01
<i>Basalt</i>	94.60	1.43	<0.01	1.08	<0.01 0.07	0.07< 0.04	<0.01	0.70	0.03	2.14	<0.01	<0.01
<i>Hi-Ca Granite</i>	94.09	1.79	<0.01	1.01	<0.01 0.02	0.02< 0.04	<0.01	0.14	0.01	3.00	0.01	<0.01
<i>Low-Ca Granite</i>	94.50	1.95	<0.01	0.89	<0.01 0.04	0.04< 0.04	<0.01	0.02	<0.01	2.69	0.02	<0.01
<i>Granodiorite</i>	94.22	1.85	<0.01	0.95	<0.01 0.02	0.02< 0.04	<0.01	0.08	0.01	2.93	0.02	<0.01

<sup>1</sup>Production is calculated using the spliced TENDL-2019 and JENDL/HE-2007 proton and neutron excitation functions (Na<sub>TJ</sub> in text). [All other Na production rates use JENDL/HE-2007 exclusively.](#)

535

Table 4

<b>Rock Type</b>	<b>Depth (m)<sup>1</sup></b>	<b>density</b>	<b><i>N</i><sub>SE</sub> (at g<sup>-1</sup>)<sup>1</sup></b>	<b><i>P</i><sub>160-FM</sub><sup>1</sup> (at g<sup>-1</sup>y<sup>-1</sup>)</b>	<b><i>P</i><sub>160</sub><sup>2</sup> (at g<sup>-1</sup>y<sup>-1</sup>)</b>
<i>Ultramafic</i>	0.18		135706	16.4	9.0
<i>Basalt</i>	0.18		132621	16.0	9.3
<i>Hi-Ca Granite</i>	0.19		148043	17.9	9.7
<i>Low-Ca Granite</i>	0.19		151127	18.3	9.9
<i>Limestone</i>	0.19		151127	18.3	10.1

<sup>1</sup>Data from Fabryka-Martin (1988), assumes SLHL production rate from oxygen in Yokoyama et al. (1977)

<sup>2</sup>Data from this study assuming only production from neutron spallation of O and an attenuation length of 160 g cm<sup>-2</sup>

|  
  
|  
  
|

Table 5

<b>Mineral</b>	<b><i>P</i><sub>M02</sub> (at g<sup>-1</sup> y<sup>-1</sup>)</b>	<b><i>P</i><sub>CDn</sub> (at g<sup>-1</sup> y<sup>-1</sup>)</b>
<i>Quartz</i>	18.72	15.37
<i>Albite</i>	17.209.99	15.4956
<i>Anorthite</i>	16.25	13.43
<i>Orthoclase</i>	16.20	13.2035
<i>Forsterite</i>	16.43	13.676
<i>Fayalite</i>	11.06	9.017
<i>Wollastonite</i>	14.42	11.85
<i>Augite</i>	14.595.91	11.853.28
<i>Ferrosilite</i>	12.804.85	10.46
<i>Enstatite</i>	17.11	14.187
<i>Calcite</i>	16.48	13.55
<i>Dolomite</i>	18.12	14.96
<b>Rock</b>		
<i>Ultramafic</i>	15.27	13.11
<i>Basalt</i>	15.38	13.72
<i>Hi-Ca Granite</i>	17.15	14.30
<i>Low-Ca Granite</i>	17.15	14.52
<i>Granodiorite</i>	17.14	14.27

540

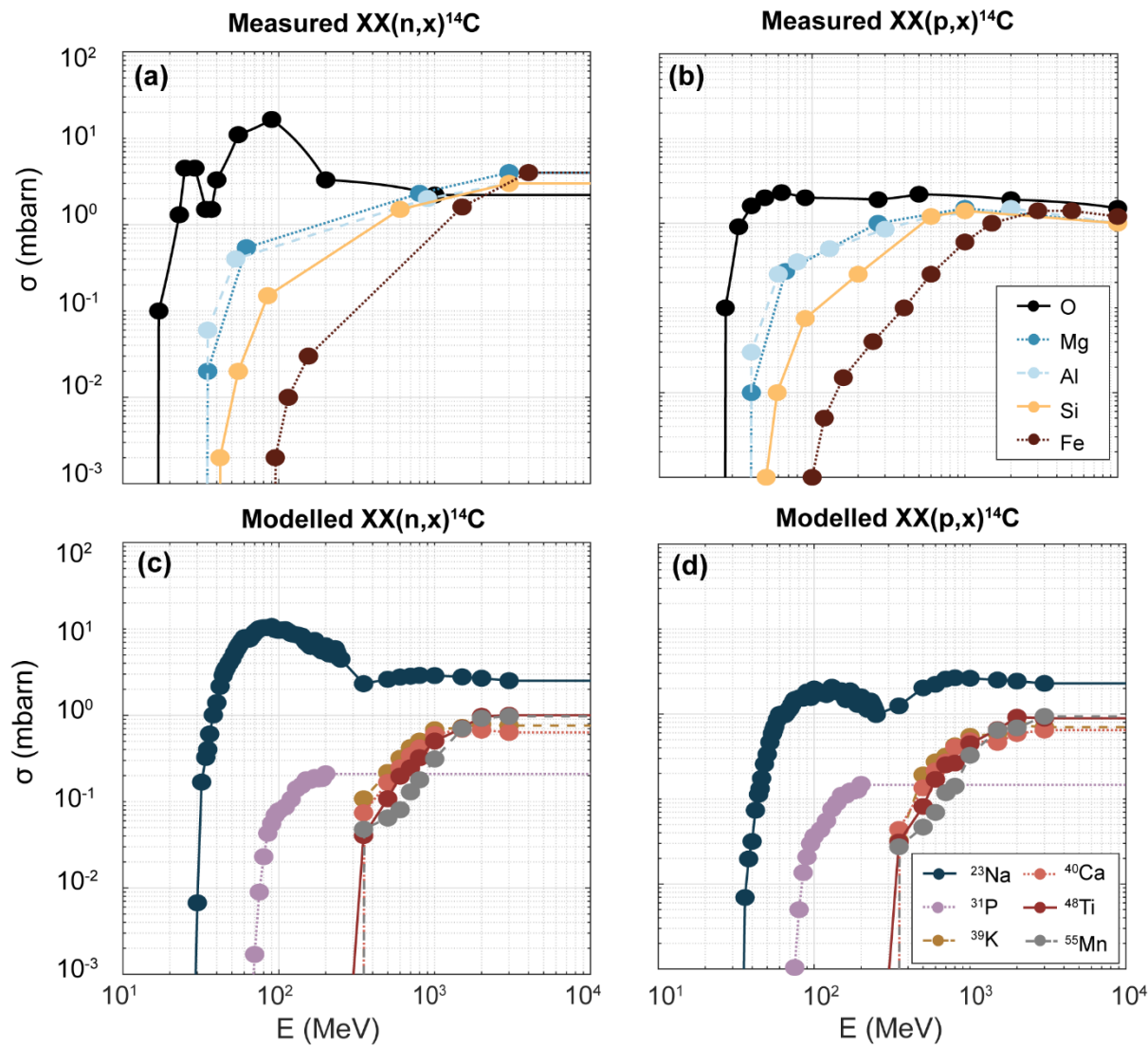


Figure 2

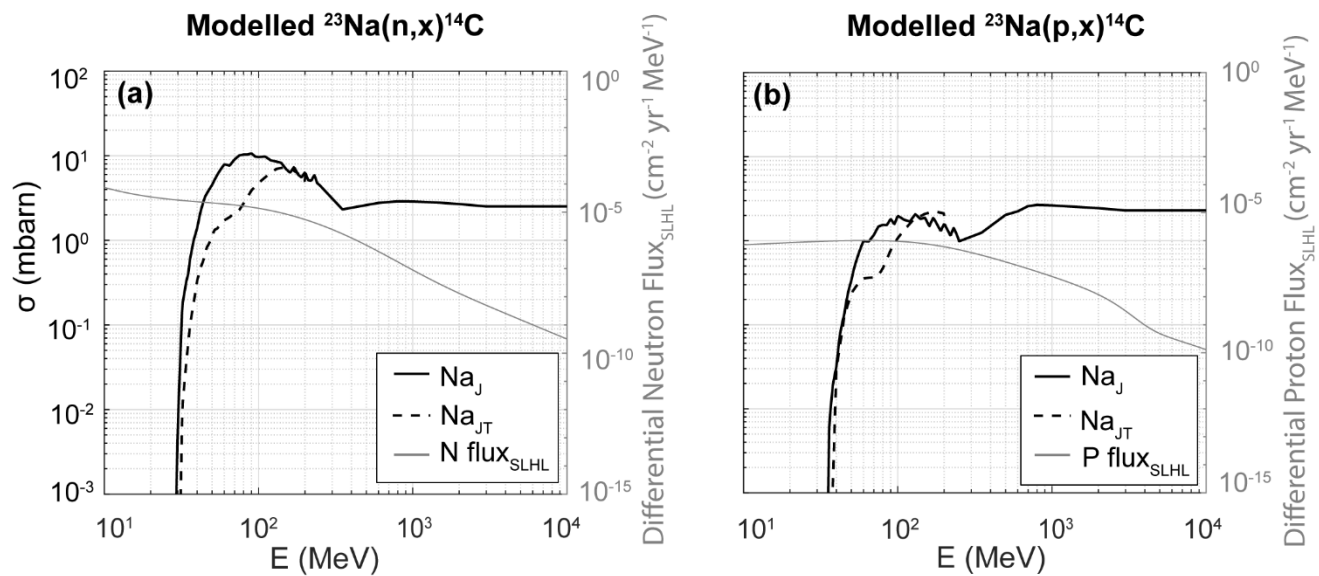
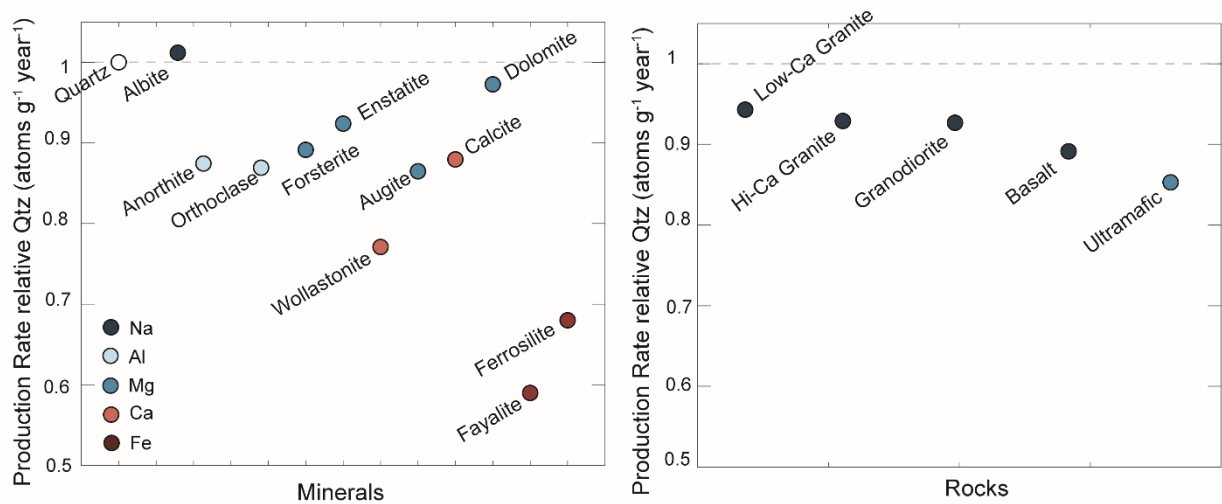


Figure 3





**Supplemental information for “A software framework for calculating compositionally dependent *in situ* <sup>14</sup>C production rates”, by Alexandria J. Koester and Nathaniel A. Lifton**

**Table S1:** *In situ* <sup>14</sup>C global calibration dataset formatted for production rate calibration input to University of Washington online calculator, version 3 (Balco et al., 2008; [http://hess.ess.washington.edu/math/v3/v3\\_cal\\_in.html](http://hess.ess.washington.edu/math/v3/v3_cal_in.html)). This dataset can be copied and pasted directly into the input data block field. Data from Borchers et al. (2016), Phillips et al. (2016), Schimmelpennig et al. (2012), and Young et al. (2014). NL gratefully acknowledges the following colleagues for providing samples from surfaces at secular equilibrium, as part of the CRONUS-Earth project (NSF EAR-0345150): Tibor Dunai (CA-05A, northern Chile), Jay Quade (SPN samples, northern Chile), John Stone (98-PCM and WBC samples, Antarctica).

05PPT-01	41.26367	-112.47527	1603	std	3	2.65	0.978	0	2005	;
05PPT-01	C-14	quartz	344740	10630	;	05PPT-01	true t	Bonneville	18300	
300	;									
05PPT-02	41.26367	-112.47527	1603	std	3	2.65	0.994	0	2005	;
05PPT-02	C-14	quartz	327590	6700	;	05PPT-02	true t	Bonneville	18300	
300	;									
05PPT-03	41.26356	-112.4758	1600	std	5	2.65	0.962	0	2005	;
05PPT-03	C-14	quartz	336220	18810	;	05PPT-03	true t	Bonneville	18300	
300	;									
05PPT-04	41.26362	-112.47693	1598	std	2.5	2.66	0.982	0	2005	;
05PPT-04	C-14	quartz	330140	8660	;	05PPT-04	true t	Bonneville	18300	
300	;									
05PPT-05	41.2639	-112.47498	1605	std	3	2.67	0.99	0	2005	;
05PPT-05	C-14	quartz	357560	11670	;	05PPT-05	true t	Bonneville	18300	300
05PPT-08	41.26379	-112.47476	1606	std	2.5	2.68	0.986	0	2005	;
05PPT-08	C-14	quartz	368590	15820	;	05PPT-08	true t	Bonneville	18300	
300	;									
06HKY-01	57.41523	-5.64637134	std	2	2.52	0.98	0	2006	;	
06HKY-01	C-14	quartz	117490	15540	;	06HKY-01	true t	Scotland	11700	300
;										
06HKY-03	57.4155	-5.64662131	std	6.7	2.47	0.981	0	2006	;	06HKY-03
06HKY-03	C-14	quartz	100780	6620	;	06HKY-03	true t	Scotland	11700	300
06HKY-04	57.42302	-5.65808137	std	4	2.59	0.956	0	2006	;	
06HKY-04	C-14	quartz	118090	7820	;	06HKY-04	true t	Scotland	11700	300
;										
06HKY-05	57.48743	-5.44933521	std	3.5	2.55	0.987	0	2006	;	
06HKY-05	C-14	quartz	144320	12210	;	06HKY-05	true t	Scotland	11700	300
;										
06HKY-06	57.48755	-5.44978527	std	3.5	2.53	0.987	0	2006	;	
06HKY-06	C-14	quartz	155910	21320	;	06HKY-06	true t	Scotland	11700	300
;										
06HKY-07	57.4878	-5.4477	500	std	6.5	2.59	0.989	0	2006	;
06HKY-07	C-14	quartz	124260	21430	;	06HKY-07	true t	Scotland	11700	300
06HKY-08	57.48863	-5.44705502	std	3	2.58	0.988	0	2006	;	
06HKY-08	C-14	quartz	146950	15000	;	06HKY-08	true t	Scotland	11700	300
;										

610	06HKY-09	57.48863	-5.44705502	std	5	2.51	0.976	0	2006	;			
	06HKY-09	C-14	quartz	140500	14950	;	06HKY-09	true t	Scotland	11700	300		
	06HKY-10	57.48732	-5.44863510	std	6	2.59	0.987	0	2006	;			
	06HKY-10	C-14	quartz	128260	19410	;	06HKY-10	true t	Scotland	11700	300		
615	06HKY-11	57.48747	-5.44995528	std	4.5	2.58	0.987	0	2006	;			
	06HKY-11	C-14	quartz	157140	14940	;	06HKY-11	true t	Scotland	11700	300		
620	MR-08-03	-43.5754551	170.60803	1029	std	2.55	2.65	0.988	0	2008	;		
	MR-08-03	C-14	quartz	227200	9000	;	MR-08-03	true t	NewZealand	9692			
		50											
	MR-08-05	-43.57434507	170.607625	1032	std	2.39	2.65	0.991	0	2008	;		
	MR-08-05	C-14	quartz	194880	8770	;	MR-08-05	true t	NewZealand	9692			
		50											
625	MR-08-13	-43.577517	170.606959	1028	std	1.41	2.65	0.991	0	2008	;		
	MR-08-13	C-14	quartz	213480	8830	;	MR-08-13	true t	NewZealand	9692			
		50											
	MR-08-14	-43.57789	170.60494	1032	std	2.35	2.65	0.991	0	2008	;		
	MR-08-14	C-14	quartz	200310	8920	;	MR-08-14	true t	NewZealand	9692			
		50											
630	11QOO-01	69.2844	-50.7569350	std	1.5	2.65	0.995	0	2011	;	11QOO-01		
	C-14	quartz	133900	8030	;	11QOO-01	true t	Greenland	9235	45	;		
	11QOO-02	69.2844	-50.7569350	std	1.5	2.65	0.995	0	2011	;	11QOO-02		
	C-14	quartz	152640	7980	;	11QOO-02	true t	Greenland	9235	45	;		
635	11QOO-03	69.2844	-50.7569350	std	1	2.65	0.995	0	2011	;	11QOO-03		
	C-14	quartz	146510	8010	;	11QOO-03	true t	Greenland	9235	45	;		
	11QOO-04	69.2844	-50.7569350	std	1.25	2.65	0.995	0	2011	;	11QOO-04		
	C-14	quartz	142790	7820	;	11QOO-04	true t	Greenland	9235	45	;		
640	11QOO-05	69.2844	-50.7569350	std	1	2.65	0.995	0	2011	;	11QOO-05		
	C-14	quartz	146970	7740	;	11QOO-05	true t	Greenland	9235	45	;		
645	DV-19	36.21825	-116.90151	69	std	4.5	2.65	0.999	0	2000	;	DV-19	
	C-14	quartz	118710	19620	;	DV-19	true t	DeathValley	50000	500	;		
	DV-18	36.2185	-116.90119	76	std	3	2.65	0.999	0	2000	;	DV-18	C-14
	quartz	135710	10210	;	DV-18	true t	DeathValley	50000	500	;			
650	DV-9	36.5272	-117.2208	480	std	4	2.65	0.999	0	2000	;	DV-9	C-14
	quartz	144350	4100	;	DV-9	true t	DeathValley	50000	500	;			
	DV-6	36.23231	-117.24528	805	std	3	2.65	0.998	0	2000	;	DV-6	
	C-14	quartz	189330	11430	;	DV-6	true t	DeathValley	50000	500	;		
655	DV-25	36.80958	-116.90952	1191	std	3	2.65	0.999	0	2000	;	DV-25	
	C-14	quartz	309670	11990	;	DV-25	true t	DeathValley	50000	500	;		
	DV-3	36.34425	-117.13612	1576	std	1	2.65	0.998	0	2000	;	DV-3	
	C-14	quartz	348130	10940	;	DV-3	true t	DeathValley	50000	500	;		
655	WHM-25	37.91078	-118.3672154	std	2	2.65	0.985	0	2000	;	WHM-25		
	C-14	quartz	490850	13330	;	WHM-25	true t	WhiteMtns	50000	500	;		
	BNR-4	37.72652	-118.57617	2337	std	3	2.65	0.975	0	2000	;	BNR-4	
	C-14	quartz	560300	9680	;	BNR-4	true t	WhiteMtns	50000	500	;		
	BNR-3	37.73315	-118.56721	2431	std	3	2.65	0.967	0	2000	;	BNR-3	
	C-14	quartz	661280	6290	;	BNR-3	true t	WhiteMtns	50000	500	;		

660	WHM-1	37.53481	-118.15325	2834	std	4	2.65	0.946	0	2000	;	WHM-
	1	C-14	quartz	779070 12440	;	WHM-1	true t	WhiteMtns	50000	500	;	
	WHM-6	37.49138	-118.16898	3200	std	4	2.65	0.944	0	2000	;	WHM-
665	6	C-14	quartz	1061480 15190	;	WHM-6	true t	WhiteMtns	50000	500	;	
	WHM-7	37.49062	-118.1712	3210	std	4	2.65	0.945	0	2000	;	WHM-
	7	C-14	quartz	1005940 17210	;	WHM-7	true t	WhiteMtns	50000	500	;	
670	WHM-11	37.55066	-118.22295	3556	std	3	2.65	0.932	0	2000	;	
	WHM-11	C-14	quartz	1139770 138490	;	WHM-11	true t	WhiteMtns	50000	500	;	
	WHM-10	37.55066	-118.22295	3556	std	5	2.65	0.932	0	2000	;	
675	WHM-10	C-14	quartz	1303710 17900	;	WHM-10	true t	WhiteMtns	50000	500	;	
	WHM-19	37.59107	-118.2412	3879	std	6	2.65	0.92	0	2000	;	
	WHM-19	C-14	quartz	1296070 17830	;	WHM-19	true t	WhiteMtns	50000	500	;	
680	WHM-15	37.59094	-118.24037	3885	std	6	2.65	0.92	0	2000	;	
	WHM-15	C-14	quartz	1272320 22010	;	WHM-15	true t	WhiteMtns	50000	500	;	
	WHM-16	37.59094	-118.24037	3885	std	6	2.65	0.92	0	2000	;	
685	WHM-16	C-14	quartz	1217980 24370	;	WHM-16	true t	WhiteMtns	50000	500	;	
	CA03-5A	-27.32	-70.7603889	224	std	4	2.65	1	0	2003	;	CA03-
	5A	C-14	quartz	110620 2060	;	CA03-5A	true t	Chile	50000	500	;	
690	SPN-699	-23.95698	-70.2858699		std	2	2.65	0.988	0	2002	;	SPN-
	699	C-14	quartz	127220 8720	;	SPN-699	true t	Chile	50000	500	;	
	SPN-977	-24.07313	-70.20565	977	std	3	2.65	0.977	0	2002	;	
695	SPN-977	C-14	quartz	210260 42600	;	SPN-977	true t	Chile	50000	500	;	
	SPN-1921	-24.47725	-69.40802	1921	std	2	2.65	0.997	0	2002	;	
	SPN-1921	C-14	quartz	331590 19490	;	SPN-1921	true t	Chile	50000	500	;	
700	SPN-3	-24.3113-68.8014333		3098	std	2.5	2.65	0.997	0	2002	;	SPN-3 C-14
	quartz	571490 19260	;	SPN-3	true t	Chile	50000	500	;			
	SPN-7D	-24.5424-68.70927		3689	std	4	2.65	0.997	0	2002	;	SPN-7D C-14
705	quartz	928560 16330	;	SPN-7D	true t	Chile	50000	500	;			
	SPN-11c	-24.56542	-68.63415	4035	std	2.5	2.7	0.997	0	2002	;	
	SPN-11c	C-14	quartz	983240 51810	;	SPN-11c	true t	Chile	50000	500	;	
710	98-PCM-010-SRDK	-70.86	68.13	225	std	3	2.7	1	0	1998	;	98-
	PCM-010-SRDK	C-14	quartz	183030 8420	;	98-PCM-010-SRDK	true t	Antarctica	50000	500	;	
	WBC-UVF	-77.75	160.8	2160	std	5	2.5	1	0	1999	;	WBC-UVF
715	C-14	quartz	968970 15770	;	WBC-UVF	true t	Antarctica	50000	500	;		
	98-PCM-002-BVLK	-70.82	68.17	100	std	3	2.8	1	0	1998	;	98-
	PCM-002-BVLK	C-14	quartz	160050 12860	;	98-PCM-002-BVLK	true t	Antarctica	50000	500	;	
720	WBC-2020	-77.75	160.8	2020	std	5.5	2.5	1	0	1999	;	WBC-2020
	C-14	quartz	974370 19180	;	WBC-2020	true t	Antarctica	50000	500	;		

[illegible]

CRONUS-A	-77.88302	160.94308	1666	std	4	2.1	0.999	0	2004	;
CRONUS-A	C-14	quartz	713510	13360	;	CRONUS-A	true t	Antarctica	50000	
500	;									

**Table S2:** Predicted modern *in situ*  $^{14}\text{C}$  spallogenic production rates (atoms  $\text{g}^{-1} \text{y}^{-1}$ ) at SLHL from neutrons and protons in minerals and rock types considered, both theoretical ( $P_{\text{CDpred}}$ ) and normalized to calibrated production in quartz ( $P_{\text{CD,GD}}$ ) using the geocentric dipolar  $R_{\text{CD}}$  record of Lifton (2016).

Mineral	Neutron $P_{\text{CDpred}}$  <i>at g<sup>-1</sup> y<sup>-1</sup></i>	Proton $P_{\text{CDpred}}$  <i>at g<sup>-1</sup> y<sup>-1</sup></i>	Total $P_{\text{CDpred}}$  <i>at g<sup>-1</sup> y<sup>-1</sup></i>	$P_{\text{CD,GD}}$  <i>at g<sup>-1</sup> y<sup>-1</sup></i>	% Diff $P_{\text{CD,GD}}$ vs. $P_{\text{Qcal}}$
<i>Quartz</i>	15.37	0.47	15.84	13.71	0.0
<i>Albite</i>	15.49	0.48	15.97	13.82	0.8
<i>Albite</i> <sup>1</sup>	14.95	0.48	15.43	13.35	-2.6
<i>Anorthite</i>	13.43	0.42	13.85	11.98	-12.6
<i>Orthoclase</i>	13.20	0.39	13.60	11.77	-14.2
<i>Forsterite</i>	13.67	0.46	14.12	12.22	-10.9
<i>Fayalite</i>	9.01	0.27	9.28	8.03	-41.4
<i>Wollastonite</i>	11.85	0.36	12.21	10.57	-22.9
<i>Augite</i>	12.00	0.37	12.38	10.71	-21.9
<i>Ferrosilite</i>	10.46	0.32	10.78	9.33	-32.0
<i>Enstatite</i>	14.18	0.46	14.64	12.67	-7.6
<i>Calcite</i>	13.55	0.38	13.94	12.06	-12.0
<i>Dolomite</i>	14.96	0.44	15.40	13.33	-2.8
<b>Rock</b>					
<i>Ultramafic</i>	13.11	0.43	13.54	11.69	-14.5
<i>Basalt</i>	13.72	0.43	14.15	12.22	-10.7
<i>Hi-Ca Granite</i>	14.30	0.44	14.75	12.73	-6.9
<i>Low-Ca Granite</i>	14.52	0.45	14.97	12.93	-5.5
<i>Granodiorite</i>	14.27	0.44	14.71	12.70	-7.1

<sup>1</sup> Production calculated using the spliced TENDL-2019 and JENDL/HE-2007 proton and neutron excitation functions (Na<sub>TJ</sub> in text). All other Na production rates use JENDL/HE-2007 exclusively.